IOP Publishing Journal of Physics: Conference Series **59** (2007) 773–777
doi:10.1088/1742-6596/59/1/165 Eighth International Conference on Laser Ablation

Nanosecond spectroscopy of expanding laser-produced tin plasma

B. O'Shay, F. Najmabadi, S. S. Harilal and M. S. Tillack

Center for Energy Research, University of California San Diego
9500 Gilman Drive, La Jolla, CA 92093-0438

Email: oshay@fusion.ucsd.edu

Abstract. Time dependent behavior of laser-produced tin plasma has been investigated using gated optical emission spectroscopy. Plasma was generated by focusing 1.064 μm Nd:YAG laser light onto a solid density, planar tin target in vacuum at a laser irradiance of 3.8×10^{11} W/cm^2. Estimates of the electron temperature and density were made by assuming Boltzmann distributed population levels and Stark broadened singly ionized tin spectral lines, respectively. An initial temperature of 1.4 eV and density of 4.1×10^{17} cm^{-3} were calculated from the analysis of spectral data. Experimental data were interpreted alongside numerical results from HYADES - a one-dimensional radiation hydrodynamics plasma simulation code. An energy balance was calculated to determine the fraction of incident laser energy converted to directed kinetic energy of expansion.

1. Introduction

Laser-produced tin plasma has been identified as one of the most energy efficient light sources for next generation extreme ultraviolet lithography (EUVL) [1,2]. In addition to meeting stringent spectral purity and energy conversion requirements, a commercial plasma based EUV lithographic light source must have a means of controlling late stage expansion debris such as energetic ions and excited neutrals. Due to extreme temperature, density, and velocity gradients within a laser-produced plasma, the characteristics of the expelled debris vary considerably over very short temporal and spatial scales. Before EUVL succeeds conventional semiconductor etching technology, the transient dynamics of the debris must be well understood.

In this paper, we report experimental results from our nanosecond spectroscopic study of laser-induced tin plasma at a laser irradiance of 3.8×10^{11} W/cm^2. While most EUVL studies have been devoted to measuring the in-band spectral radiation, this work is unique in that it focuses on the cooler visible emissions, characteristic of the late time plasma behavior. Through optical emission spectroscopy we diagnosed the time evolution of the fundamental plasma quantities driving the hydrodynamic expansion of the tin plume; *viz*., electron temperature and density. Excitation temperature was obtained by invoking local thermodynamic equilibrium (LTE) arguments and generating Boltzmann diagrams, while electron density was estimated from Stark broadening theory. These data can be used to help predict ion energies

© 2007 IOP Publishing Ltd

and flux values at various distances from the target in future EUVL systems. Numerical simulations were performed to guide and interpret our experimental data. An energy partition was calculated to determine the relative fractions of plasma thermal, kinetic, and radiative energy, as well as to provide insight into the mechanisms of their exchange for the duration of the event. An energetics analysis allows us to quantify the risk of highly energetic plasma species to EUV focusing optics in a projection lithography device.

2. Experimental arrangement and diagnostics

The experimental procedures utilized in this work have been described in greater detail elsewhere [3]. Briefly, plasma was created by focusing 1.064 μm light from a Q-switched (10 ns FWHM) Nd:YAG laser onto a 98.8% pure 2 mm thick planar tin target. A 58 ± 3 μm $1/e^2$ focal spot diameter was measured using an accurate optical imaging technique that will be discussed in a future publication. Laser beam energy was monitored with a thermal volume absorber and set to 100 mJ, providing an overall laser irradiance of $3.8 \pm 0.4 \times 10^{11}$ W/cm^2.

The plasma's emission spectrum was measured by observing the plasma orthogonally to the target surface. A one-to-one optical imaging system comprising two f = 35 cm plano-convex lenses and a 3" diameter enhanced Al mirror collimated and refocused visible emission onto the 20 μm entrance slit of a 0.5 m Czerny-Turner spectrograph (Acton, Spectra-Pro 500i). The three optic system was translated along the expansion direction using a micrometer driven stage to spatially sample various parts of the plume (±5 μm uncertainty) while maintaining central focus on the entrance slit. The exit port of the spectrograph was coupled to a gateable, intensified CCD camera (Princeton Insts. ICCD, PI-MAX Model 512 RB, 1.6 ns FWHM resolution) operated with vertical binning of the CCD array to obtain spectral intensity vs. wavelength. A programmable timing generator enabled the acquisition of time resolved plasma spectra by controlling the delay between laser pulse arrival and the detector system, as well as the intensification (exposure) time. For temperature and density measurements, the gate width of the intensifier was set to 10 and 25 ns, respectively.

3. Modeling

Plasma simulations were performed using HYADES – a one-dimensional, three-temperature, three-geometry radiation hydrodynamics and energy transport code [4]. HYADES was operated in cylindrical geometry mode, and the ionization balance was determined using a Saha model where ionization and recombination processes exactly balanced one another. Radiative transfer was treated in the flux-limited gray radiation diffusion approximation using tabular Rosseland and Planck mean opacities. Thermodynamic and equation of state properties were derived from the LANL Sesame tables.

4. Results

4.1. Experiment

Time resolved spectroscopic measurements of the Stark broadened singly ionized $\lambda = 556.2$ nm ($6d^2D \rightarrow 6p^2P^o$) Sn spectral line were used to calculate the electron density. In the electron impact approximation to pressure broadening, the width of the line profile is linearly proportional to the perturber density [5]. Numerical fits of experimental data to theoretical Lorentzian line profiles exhibited a high degree of symmetry indicating that the ion broadening component was negligible [6].

The excitation temperature was obtained by the widely accepted Boltzmann diagram method, where the emission intensities of 5 spectral lines were related to their temperature dependent excited level population distributions. This technique assumes that atomic processes in the plasma are dominated by collisional rather than radiative transitions so that Boltzmann statistics may be applied [7]. The spectral

lines selected for the Boltzmann plot were 684.4 nm ($6p^2P^o \rightarrow 6s^2S$), 645.4 nm ($6p^2P^o \rightarrow 6s^2S$), 558.9 nm ($4f^2F^o \rightarrow 5d^2D$), 556.2 nm ($6d^2D \rightarrow 6p^2P^o$), and 533.2 nm ($6d^2D \rightarrow 6p^2P^o$).

Figures 1 and 2 below show the temporal evolution of electron temperature and density of tin plasma measured at 0.75, 1, and 2 mm from the target. Reliable data could only be acquired for distances ≥ 0.75 mm from the target where spectral lines began to emerge from the continuum. At 0.75 mm and ~85 ns after laser light impinged upon the target, a peak electron temperature of 1.4 eV and density of 4.1×10^{17} cm^{-3} were observed. Plasma temperatures at 0.75 and 1 mm from the target were similarly behaved and exhibited a weak dependence upon time. The temporal delay between peak temperatures at successive spatial points is due to the time of arrival of the core plasma at the given location. The ascending limb in the temperature data is more prominent for distances > 0.75 mm simply because the continuum obscures the spectral lines near the target. The density decay rate decreased with increasing distance from the target due to the relaxation of initially large pressure gradients within the plume. From analysis of the time resolved λ = 556.2 nm spectral line used for density measurement, a most probable expansion velocity of $1.9 \pm 0.9 \times 10^6$ cm/sec (kinetic energy ~ 220 eV) was determined for the singly ionized tin debris. It should be noted that this technique does not account for the origins of the Sn II excited state.

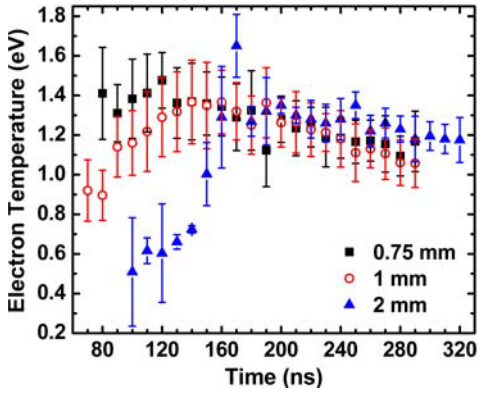

FIG. 1. Temporal evolution of plasma temperature at sequential distances from target. Error bars due to least squares fit to measurements made at multiple wavelengths.

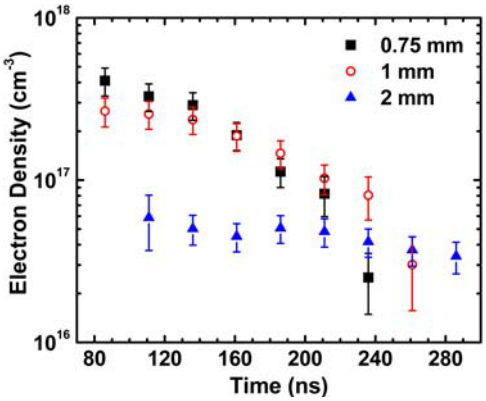

FIG. 2. Temporal evolution of electron density at sequential distances from target. Error bars due to uncertainty in electron impact parameter and theoretical fit to Lorentzian profile.

4.2. Simulations

Due to the plane wave nature of the laser source in HYADES, an input laser intensity of ½ of the experimental value was specified. Time resolved electron temperature and density from HYADES are plotted in Figures 3 and 4, respectively at 0.75, 1, and 2 mm from the target. The code generally predicts hotter, denser plasma conditions than were measured experimentally. The reasons for this are most likely due to the limited capability of a one-dimensional code in modeling a multi-dimensional expansion.

In an effort to validate the energetics of the model, we compared the time evolution of numerical and experimental energy densities at a distance of 0.75 mm from the target. This position was chosen because it represents the most dynamic region of the plasma (within our dataset), and would therefore provide an upper bound on the deviations from numerical results. On average, the data in Figure 5 show that the model predicts more thermal but less kinetic energy than what was measured experimentally. The figure inset, which is the integral of the sum of the thermal and kinetic components from the main plot, suggests

that in spite of the discrepancies observed between experiment and model in Figures 1-4, HYADES is capable of recovering the overall plasma energy to within a factor of 2.

To understand the time dependent flow of energy within the plasma, we investigated the various forms in which the energy could reside using HYADES. As shown in Figure 6, the plasma radiates away ~90% of the absorbed laser energy during the pulse. Once the laser has been switched off at ~25 ns, plasma radiation losses are negligible. At this time, the ratio of kinetic to escaped radiative energy is a factor of ~25, indicating that the plasma expansion is adiabatic. Immediately after the laser, the kinetic energy makes up more than 50% of the energy remaining in the system, rising steadily to 85% at 300 ns. The increase in material kinetic energy occurs by direct conversion from electron thermal energy. The relatively hot electrons have a sizeable pressure compared to the ions, and do pdV work on the ion population as they cool.

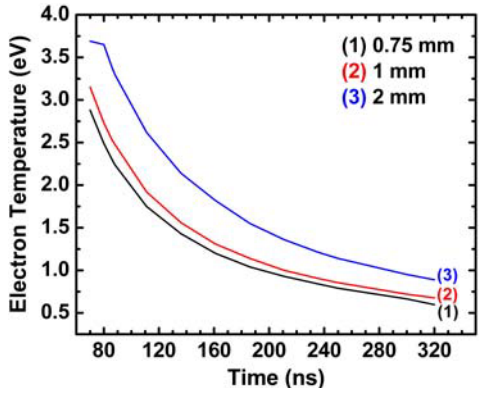

FIG. 3. Temporal behavior of electron temperature at various positions obtained from numerical model.

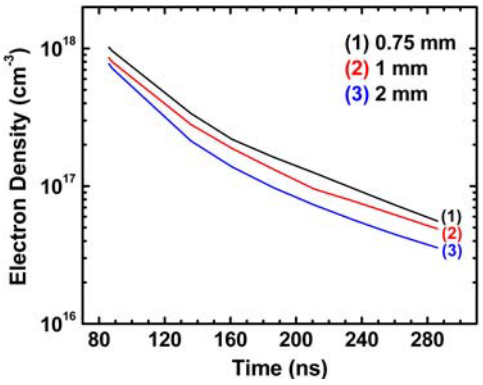

FIG. 4. Temporal behavior of electron density at various positions obtained from numerical model.

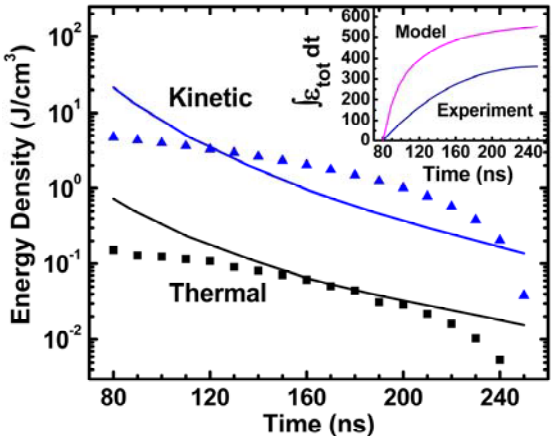

FIG. 5. Time evolution of thermal and kinetic energy densities at 0.75 mm from target. Experimental data are shown as points and model results as solid lines. The figure inset shows the total time integrated experimental and numerical energy densities.

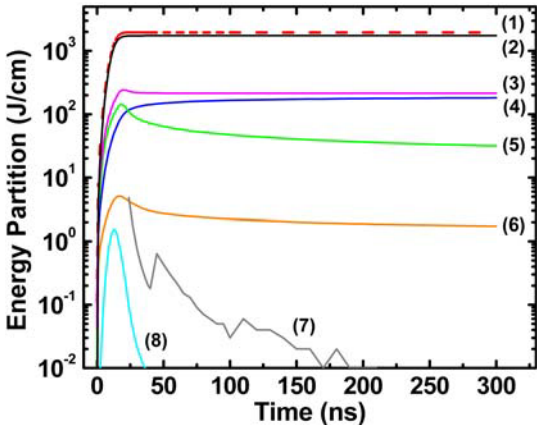

FIG. 6. Time dependent energy partition for Sn plasma: (1) cumulative absorbed laser energy; (2) cumulative escaped radiation; (3) total energy – radiation losses; (4) kinetic energy; (5) electron energy; (6) ion energy; (7) post laser radiation losses; (8) radiation internal energy.

In an EUVL system, the directed ions pose the greatest threat to the survival of nearby optics. The fact that these simulations suggest a ~9% conversion efficiency between laser and ion kinetic energy, coupled with our experimental measurement of 220 eV ions demonstrates the need for continued study of target debris and its mitigation. We are presently exploring the efficacy of steady state magnetic fields and transparent buffer gases in shifting the ion spectrum to lower energies.

References

[1] Marx, B 2003 *Laser Focus World* **39**(4) 34
[2] Spitzer R C, Kauffman R L, et al. 1993 *J. Vac. Sci. Technol.* B **11**(6) 2986-2989
[3] Harilal S S, O'Shay B, et al. 2005 *J. Appl. Phys.* **98**(1) 013306
[4] Larsen, J T and Lane, S M 1994 *JQSRT* **51**(1-2) 179-186
[5] Baranger, M 1958 *Physical Review* **111**(2) 481-493
[6] Griem, H R 1974 *Spectral Line Broadening by Plasmas* (New York: Academic Press)
[7] Griem, H R 1997 *Principles of Plasma Spectroscopy* (Cambridge: Cambridge University Press)